ACCURACY ASSESSMENT OF NUMERICAL TRACING OF THREE-DIMENSIONAL MAGNETIC FIELD LINES IN TOKAMAKS WITH ANALYTICAL INVARIANTS

R. ALBANESE,[a,b]* M. DE MAGISTRIS,[a,b] R. FRESA,[a,c] F. MAVIGLIA,[a,b] and S. MINUCCI[a,b]

[a]*Consorzio CREATE, Naples, Italy*
[b]*Università di Napoli FEDERICO II, Dip. di Ingegneria Elettrica e delle Tecnologie dell'Informazione (DIETI), Naples, Italy*
[c]*Università della Basilicata, Scuola di Ingegneria, Potenza, Italy*

Received December 16, 2014
Accepted for Publication February 25, 2015
http://dx.doi.org/10.13182/FST15-127

We consider the problem of the accurate tracing of long magnetic field lines in tokamaks, which is in general crucial for the determination of the plasma boundary as well as for the magnetic properties of the scrape-off layer. Accurate field line tracing is strictly related to basic properties of ordinary differential equation (ODE) integrators, in terms of preservation of invariant properties and local accuracy for long-term analysis. We introduce and discuss some assessment criteria and a procedure for the specific problem, using them to compare standard ODE solvers with a volume-preserving algorithm for given accuracy requirements. In particular, after the validation for an axisymmetric plasma, a three-dimensional (3-D) configuration is described by means of Clebsch potentials, which provide analytical invariants for assessing the accuracy of the numerical integration. A standard fourth-order Runge-Kutta routine at fixed step is well suited to the problem in terms of reduced computational burden, with extremely good results for accuracy and volume preservation. Then we tackle the problem of field line tracing in the determination of plasma-wall gaps for a 3-D configuration, demonstrating the effective feasibility of the plasma boundary evaluation in tokamaks by tracing field lines with standard tools.

KEYWORDS: *magnetic field line tracing, plasma boundary, volume-preserving numerical algorithms*

Note: Some figures in this paper may be in color only in the electronic version.

I. INTRODUCTION

Basic equilibria in tokamaks are mostly two-dimensional (2-D) axisymmetric, whilst the three-dimensional (3-D) perturbations are considered in different contexts, mainly related to plasma stability and control. Three-dimensional effects are associated with magnetohydrodynamic activity, plasma instabilities (e.g., resistive wall modes, neoclassical tearing modes, and edge localized modes), and nonaxisymmetric control coils; however, 3-D magnetic fields are also produced during normal operation by the eddy currents induced in the 3-D metallic structures, not to mention the ripple of the toroidal field and the error fields. Therefore, when realistic estimations of 3-D parameters have to be carried out (shape, scrape-off layer, connection length, wall

*E-mail: raffaele.albanese@unina.it

loads, etc.), an accurate tracing of magnetic field lines is required.[1–7]

Once the field is known, in either analytical or numerical form, the problem is easily recognized as the tracing of a vector field flow, which turns it into the solution of a given ordinary differential equation (ODE) set. The problem, in principle trivial, is actually challenging due to the typical very long magnetic lines needed to trace accurately at an affordable computational cost.[8] The length of typical lines to be traced is $\sim 10^3$ m, with a required accuracy of 10^{-3} m, so achieving a factor 10^{-6} in relative precision over the entire integration length.

The problem of the long-term behavior in ODE sets is faced in several science areas, e.g., in classical nonlinear dynamics for the determination of bifurcation diagrams and chaotic attractors. Thus, much effort has been devoted to improving the properties of the algorithms, mainly for the so-called geometric integrators.[9–13] In these cases, the main interest is in the preservation of some average properties of the solution. On the other hand, if the plasma geometry has to be determined in tokamaks, the accuracy of every single line traced is crucial for a reliable estimation of the quantities under investigation. The main aim of this paper is to discuss the performance and results of some ODE integrators for 3-D field line integration in tokamaks. In particular, this paper largely extends methods and results reported by Albanese et al.,[14] by introducing a new full 3-D assessment scheme based on a magnetic field representation using Clebsch potentials.

This paper is organized as follows. Section II illustrates in general the problem of **B**-field line tracing formulated as the solution of a divergence-free ODE equation, and then it details the implementation of a volume-preserving (VP) integration scheme. In Sec. III, we introduce and discuss some criteria for comparing algorithms, with reference to the typical tokamak field structure for both axisymmetric and full 3-D cases; the implemented VP algorithm is then compared to standard ODE Runge-Kutta routines, with overall performance of the latter being favorable. In Sec. IV, the Runge-Kutta algorithm is viably and successfully used to calculate plasma-wall gaps with a 3-D line-tracing scheme.

II. FIELD LINE EVALUATION

The problem of tracing field lines with an assigned magnetic flux density field **B** is equivalent to the tracing of a velocity flow **v** for incompressible fluids in stationary conditions, due to the common divergence-free property of both vector fields ($\nabla\cdot\mathbf{v} = 0 \leftrightarrow \nabla\cdot\mathbf{B} = 0$). As such, it can be formulated as the solution of an ODE flow,

$$d\mathbf{x}/d\tau = \mathbf{B}(\mathbf{x}) \ , \tag{1}$$

from a specified starting point $\mathbf{x}_0$ at $\tau = 0$, where $\mathbf{B}(\mathbf{x})$ is the magnetic flux density field in terms of the position **x** (we consider stationary magnetic configurations). Therefore, once the required spatial resolution in the mapping of the plasma boundary is assigned, an accurate solution of Eq. (1) is needed, also for very long integration lengths, at an affordable computational burden.

The problem can be faced with standard ODE integrators, but strict control and verification of the integration error is needed to ensure reliable results in its application, for example, in 3-D plasma shape reconstructions. Moreover, it is highly desirable that intrinsic invariant properties, such as the divergence-free structure of the field, are preserved in the numerical solution. Indeed, correct integration of Eq. (1) is VP, like for Lagrangian trajectories in incompressible fluids. Such invariance can be used, a posteriori, as a figure of merit of the integrator accuracy. In this paper, we consider classical schemes, such as Runge-Kutta of second order (RK-II) and fourth order (RK-IV).

A different approach is the implementation of VP integration schemes that a priori guarantee the volume invariance.[9–11] In particular, we implemented a vector potential splitting method, which belongs to the class of generating function algorithms.[9] It is based on splitting the 3-D **B** field as the sum of 2-D divergence-free components, as properly obtained from a vector potential $\mathbf{B} = \nabla \times \mathbf{A}$ (with the Coulomb gauge) and their integration via any symplectic method, so preserving the volume. By expressing both the flux density field and the vector potential in Cartesian components, it is possible to consider the splitting $\mathbf{B} = \mathbf{B}_1 + \mathbf{B}_2 + \mathbf{B}_3$ with

$$\mathbf{B}_1 = \nabla A_x \times \mathbf{i}_x \ ,$$
$$\mathbf{B}_2 = \nabla A_y \times \mathbf{i}_y \ ,$$

and

$$\mathbf{B}_3 = \nabla A_z \times \mathbf{i}_z \ . \tag{2}$$

Each $\mathbf{B}_i$ component is 2-D (the stream function $\mathbf{B}_i$ of the i'th ODE set has no component along one axis; e.g., $\mathbf{i}_x\cdot\mathbf{B}_1 = 0$), and the corresponding ODE set is Hamiltonian, with A_i the Hamiltonian function. As a consequence, each $\mathbf{B}_i$ field is divergence-free; thus, the ODE set can be integrated with a symplectic/area-preserving numerical integrator, ensuring the preservation of the solenoidal structure of the given ODE flow. For such a problem, the midpoint rule (MR) method with step h,

$$\mathbf{x}_{i,k+1} = \mathbf{x}_{i,k} + h\mathbf{B}_i\left(\frac{\mathbf{x}_{i,k+1} + \mathbf{x}_{i,k}}{2}\right) \ , \tag{3}$$

where $\mathbf{x}_{i,k}$ and $\mathbf{x}_{i,k+1}$ are the positions at steps k and k+1 related to integration of the i'th component $\mathbf{B}_i$ of the field, is symplectic (area preserving).[10] This can be easily verified by writing Eq. (3) in explicit form as

$$\mathbf{x}_{i,k+1} = \Im_{i,k+1}(\mathbf{x}_{i,k}, h) \ . \tag{4}$$

Fusion Science and Technology fstfst15-127.3d 1/10/2015 18:46:17

Note that the associated Jacobian matrix $\mathbf{J}_i$ (where the subscript i identifies the corresponding field component),

$$\mathbf{J}_i = \frac{\partial \mathbf{x}_{i,k+1}}{\partial \mathbf{x}_{i,k}} = \left(1 - \frac{h\mathbf{F}_i}{2}\right)^{-1}\left(1 + \frac{h\mathbf{F}_i}{2}\right), \text{ with}$$
$$\mathbf{F}_i = \frac{\partial \mathbf{B}_i}{\partial \mathbf{x}_{i,k}} \ , \tag{5}$$

has unitary determinant, since $Tr(\mathbf{F}_i) = \nabla\cdot\mathbf{B} = 0$:

$$\det(\mathbf{J}_i) = \frac{1 + \frac{h}{2}Tr(\mathbf{F}_i) + \frac{h^2}{4}\det(\mathbf{F}_i)}{1 - \frac{h}{2}Tr(\mathbf{F}_i) + \frac{h^2}{4}\det(\mathbf{F}_i)}$$
$$= \frac{1 + \frac{h^2}{4}\det(\mathbf{F}_i)}{1 + \frac{h^2}{4}\det(\mathbf{F}_i)} = 1 \ . \tag{6}$$

Note that the sorted composition of the three 2-D fields,

$$\mathbf{x}_{k+1} = \mathbf{x}_{3,k+1} = \Im_{1,k+1}(\mathbf{x}_{i,k},h)^{\circ}\Im_{2,k+1} \times (\mathbf{x}_{1,k+1},h)^{\circ}\Im_{3,k+1}(\mathbf{x}_{2,k+1},h) \ , \tag{7}$$

is a 3-D VP mapping because the associated determinant is the product of the unitary determinants associated with each i'th integration substep in Eq. (3). This formula defines a first-order accuracy algorithm; a second-order accuracy multistep algorithm can be obtained via five 2-D transformations:

$$\mathbf{x}_{k+1} = \mathbf{x}_{5,k+1} = \Im_{1,k+1}(\mathbf{x}_{i,k},h/2)^{\circ}\Im_{2,k+1} \times (\mathbf{x}_{1,k+1},h/2)^{\circ}\Im_{3,k+1}(\mathbf{x}_{2,k+1},h)^{\circ}\Im_{2,k+1} \times (\mathbf{x}_{3,k+1},h/2)^{\circ}\Im_{1,k+1}(\mathbf{x}_{4,k+1},h/2) \ . \tag{8}$$

We set up a MATLAB procedure based on the above ODE integration schemes, providing a tool for the tracing of 3-D field lines in tokamaks. Figure 1 shows an example of its graphical output for a kinked plasma configuration.

III. ACCURACY ASSESSMENT AND CLEBSCH POTENTIALS

The principal aim of this section is to discuss and compare the performance of standard ODE algorithms based on the Runge-Kutta method with the VP-MR scheme of Eq. (3) (Ref. 15).

The error assessment for such a problem in a tokamak is not trivial because

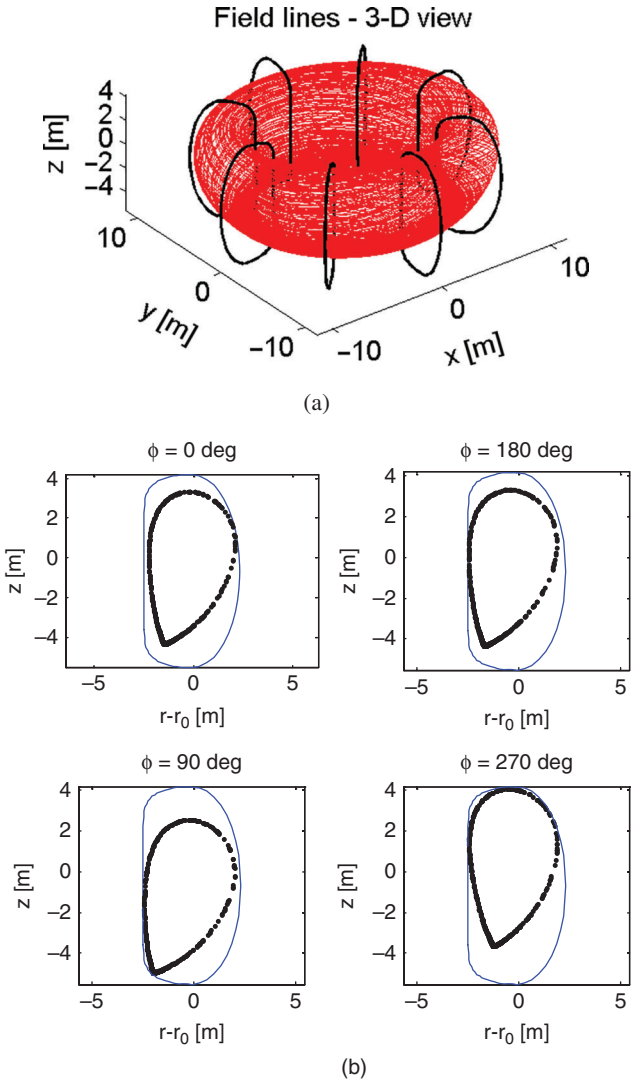

Fig. 1. Plot of field lines of a perturbed plasma: (a) 3-D view; (b) Poincaré cross sections at fixed toroidal angles.

1. for accurate tracing, the error has to be bounded after a long integration
2. analytical invariants for plasma equilibria, such as the poloidal magnetic flux Ψ, are usually available only for the 2-D axisymmetric case
3. the transverse (poloidal plane) components of the field (and therefore the related error) are usually much smaller than the toroidal one.

A first error estimation of these 3-D integrators can be given just considering an axisymmetric plasma configuration,[14] by evaluating for such a case the precision of the poloidal magnetic flux Ψ, and the conservation of the Jacobian of the mapping in the 3-D integration of the field. Such an estimation follows the conjecture that the combination of high accuracy in flux evaluation (related to the poloidal component in the 2-D

Fusion Science and Technology fstfst15-127.3d 1/10/2015 18:46:17

axisymmetric case) with high volume preservation in the 3-D integration guarantees good accuracy also for longitudinal components.

Following such an approach, a DEMO configuration (plasma current $I_p = 16$ MA, major radius $R_0 = 9$ m, minor radius $a = 2.25$ m, poloidal beta $\beta_p = 0.8$, plasma internal inductance $l_i = 0.7$, and toroidal field of 7 T at R_0) is considered and **B**-field lines 1 km long within the plasma are traced[16]; then the considered algorithms are tested in terms of accuracy and computation time as functions of the integration step size in a cylindrical coordinate system. Figure 2 shows the relative error in terms of $\Delta\Psi/\Psi$, for different integration step lengths, whereas in Fig. 3 we illustrate the relative variation of the Jacobian determinant as a function of the curvilinear abscissa over the field line. The observed periodic behavior is explained for the axisymmetry of the configuration, after one complete turn in the poloidal plane is made. The local VP condition, $|J|-1 = 0$, verified at the round-off error limit, stays within an accuracy of 10^{-10} for both the MR rule and the RK-IV scheme. For the latter, this gratifying result is mainly due to the small integration step selected for accuracy requirements.

Note that the relative error $\Delta\Psi/\Psi$ in the evaluation of the magnetic flux scales with the integration step in perfect agreement with the algorithm order (Fig. 2), as proof that the considered integration step sizes are large enough to consider round-off errors negligible with respect to truncation error.

To evaluate the numerical accuracy in volume preservation of the considered integration schemes, one has to consider that the Jacobian matrix, Eq. (5), whose entries consist of partial derivatives, can be numerically calculated by a central-point derivation rule with a

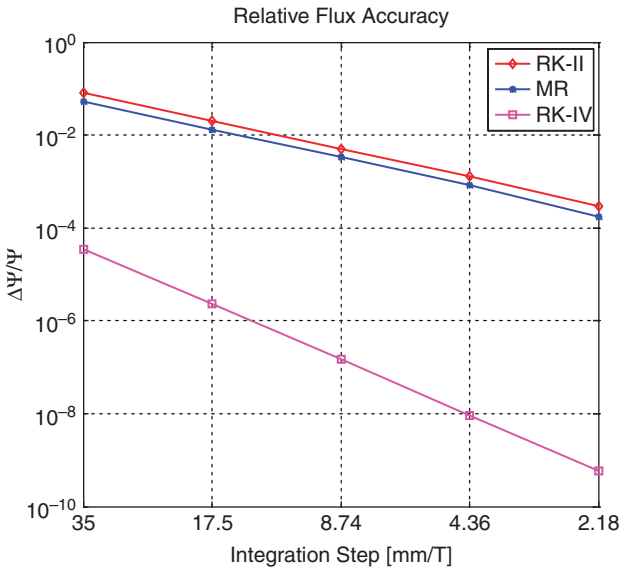

Fig. 2. Flux accuracy in terms of integration step length for the considered algorithms: MR, RK-II, and RK-IV.

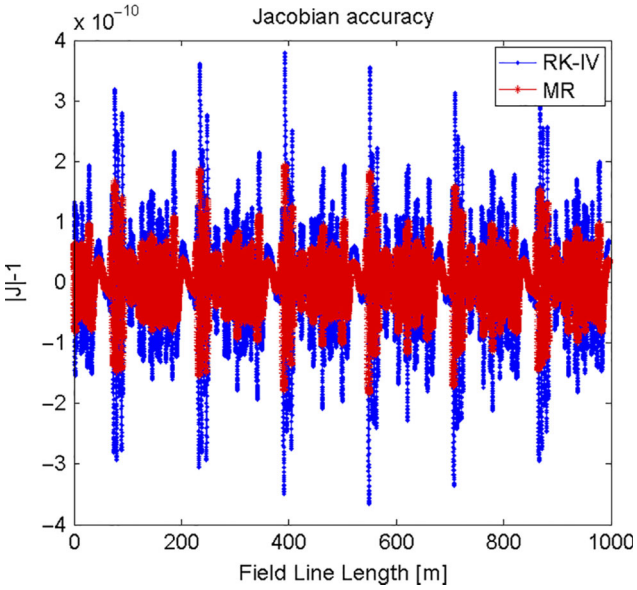

Fig. 3. Volume-preserving condition along the integration for MR and RK-IV at the truncation error limit.

second-order approximation. Therefore, the accuracy can be evaluated with a second-order extrapolation as

$$\frac{J(\tau)}{J(0)} = 2\frac{J_{\frac{h}{2}}(\tau)}{J_{\frac{h}{2}}(0)} - \frac{J_h(\tau)}{J_h(0)} + O[h^2] \,, \tag{9}$$

where $J = \det(\mathbf{J}_i)$ is the Jacobian determinant and h indicates the step size for the numerical calculation of the partial derivatives. As a result we get, for $h = 320$ μm, the accuracies of $|J|-1 = 0$ as 0.460×10^{-12} for MR and 3.302×10^{-12} for RK-IV.

In Table I, a general comparison of the considered algorithms is given in terms of flux accuracy and computing time.

A fully 3-D tracing accuracy assessment can be developed by observing that 3-D invariants can be found using the Clebsch decomposition for the magnetic fields. Such a representation expresses a divergence-free field as the cross product of the gradients of two scalar functions as

$$\mathbf{B} = \nabla U \times \nabla V \,. \tag{10}$$

This representation is used in the description of the magnetic field lines as a Hamiltonian flow.[17] In Eq. (10), the two Clebsch potentials U and V label magnetic surfaces ($\mathbf{B}\cdot\nabla U = 0$ and $\mathbf{B}\cdot\nabla V = 0$), so a magnetic field line is given by the intersection of two surfaces: U = constant and V = constant.

Using such fundamental properties, a first basic estimate of the accuracy in the numerical tracing of 3-D magnetic field lines can be obtained by evaluating the relative error on the U and V potentials along the traced field lines. To turn such information into a geometrical error, it is possible to calculate the minimal distance

Fusion Science and Technology fstfst15-127.3d 1/10/2015 18:46:17

TABLE I

Flux Accuracy for MR and RK with Respect to the Integration Step for an Integration Length of 1000 m

$\Delta\tau$ (mm/T)	MR	RK-II	RK-IV
35.0			
$\Delta\Psi$ (V·s)	0.911	1.382	5.986e−4
CPU time (s)	239	60	116
17.5			
$\Delta\Psi$ (V·s)	0.225	0.346	3.907e−5
CPU time (s)	480	118	241
8.72			
$\Delta\Psi$ (V·s)	0.057	0.087	2.492e−6
CPU time (s)	923	245	489
4.36			
$\Delta\Psi$ (V·s)	0.014	0.022	1.574e−7
CPU time (s)	1594	493	990
2.18			
$\Delta\Psi$ (V·s)	0.003	0.005	9.876e−9
CPU time (s)	2749	996	1992

$\|\delta P\|_{\min}$ between the exact field line $U = U_0 \cap V = V_0$ and the actual numerical line by solving in the least-squares sense the underdetermined set:

$$\nabla U \cdot \delta P = U - U_0$$

and

$$\nabla V \cdot \delta P = V - V_0 \ , \tag{11}$$

where U and ∇U, and V and ∇V are the actual values of the Clebsch potentials with their gradients at the points of the computed field line; U_0 and V_0 are the corresponding values of the Clebsch potentials on the analytical field line.

Considering the parametric equations of a toroidal helix, we choose the Clebsch potentials in such a way that the corresponding field configuration resembles the field of a typical axisymmetric plasma:

$$U = \frac{(r - R_0)^2}{a^2} + \frac{(z - Z_0)^2}{b^2} + U_0$$

and

$$V = \theta - \frac{\varphi}{q} + V_0 \ , \tag{12}$$

where R_0 and Z_0 are the poloidal coordinates of the center of the elliptic cross section of the helix, whose axes are a and b; q is the safety factor; φ is the toroidal angle; θ is obtained from $(r - R_0)\tan(\theta) = z - Z_0$ using the four-quadrant inverse tangent formula; and U_0 and V_0 are arbitrary constants.

Figure 4 shows two surfaces, U = constant and V = constant, defined by Eq. (12); their intersection is a toroidal helix confined inside the vacuum vessel.

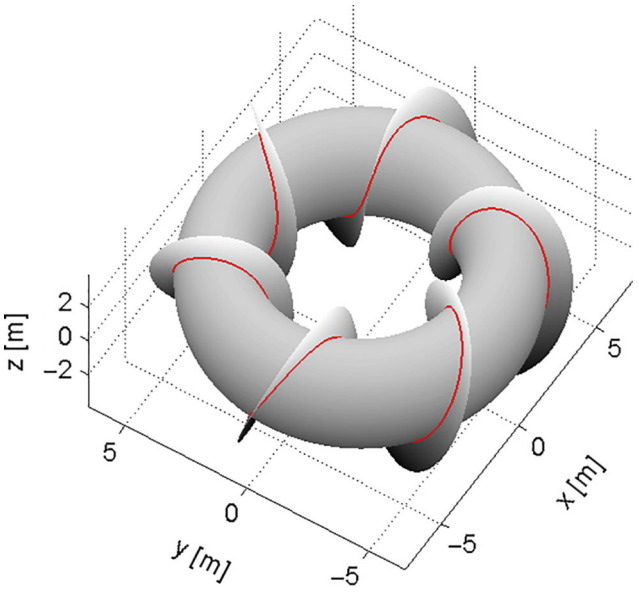

Fig. 4. Clebsch surfaces generating a toroidal helix (the solid line shows the intersection of the two surfaces).

Such an axisymmetric field configuration can be easily modified by adding proper perturbing nonaxisymmetric terms in the expressions of U and V. In the following, two kinds of perturbation will be considered, namely, a global perturbation and a local perturbation.

With regard to the global perturbation, a mode resembling the typical ripple field is given as

$$U = \frac{(r - R_0)^2}{(a + \delta U)^2} + \frac{(z - Z_0)^2}{(b + \delta U)^2} - 1 \ ,$$
$$\delta U = \delta r \cos(n\varphi) \ ,$$

and

$$V = \theta - \frac{\varphi}{q} + V_0 \tag{13}$$

and is shown in Fig. 5 for $R_0 = 9$ m, $Z_0 = 0$, $a = 0.75$ m, $b = 1.25$ m, $q = 2\pi$, $\delta r = 0.25$ m, and $n = 18$.

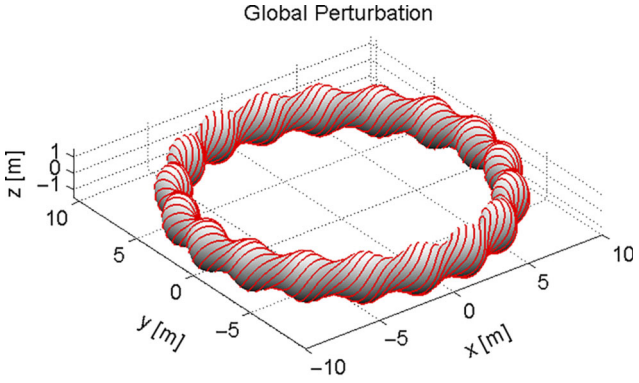

Fig. 5. Ergodic surface covered by a field line in a globally perturbed field configuration.

Again, for the Jacobian conservation condition, we carry out the same extrapolation as for the axisymmetric test case obtaining the accuracies for $|J|-1 = 0$ as 0.4918×10^{-11} for the MR and 0.3190×10^{-11} for the RK-IV algorithms.

For the local perturbation, we consider the following (Fig. 6), obtained by adding a smooth function $\delta U \subset \Omega_p$ to the unperturbed field:

$$U = \frac{(r - R_0 - \delta U)^2}{a^2} + \frac{(z - Z_0)^2}{b^2} - 1 \ ,$$

$$\delta U = \delta r \cdot e^{\dfrac{a_1}{\Delta z} - \dfrac{a_1}{\sqrt{\Delta z^2 - (Z_1 - z)^2}}} \times e^{\dfrac{\alpha}{\Delta\varphi} - \dfrac{1}{\sqrt{\Delta\varphi^2 - (\varphi_1 - \varphi)^2}}} u(r - R_0) \ \text{ in } \ \Omega_p$$

$$\text{and } 0 \text{ elsewhere} \ ,$$

and

$$V = \theta - \frac{\varphi}{q} + V_0 \ , \tag{14}$$

with $R_0 = 9$ m, $Z_0 = 0$, $a = 0.75$ m, $a_1 = 10$ m, $b = 1.25$ m, $\alpha = 1$ rad, $q = 2\pi$, $\delta r = 1$ m, $\Delta z = 0.5$ m, $X_1 = 1.56$ m, $Y_1 = 8.86$ m, $Z_1 = Z_0$, $\Delta\varphi = 20$ deg, $\varphi_1 = -90$ deg, and

$$\Omega_p = \left\{ \begin{array}{c} |z| \leq z_1 \\ |\varphi - \varphi_1| \leq \Delta\varphi \end{array} \right\} . \tag{15}$$

Table II shows the accuracy assessments both in the axisymmetric and in the two full 3-D configurations mentioned above, for the MR, RK-II, and RK-IV algorithms.

This analysis suggests that standard integrators, e.g., Runge-Kutta, are extremely accurate in terms of volume preservation (basically at the limit of round-off), when selecting appropriate accuracy requirements (step size). At the same time, they are by far simpler and less expensive than VP algorithms from a computational point

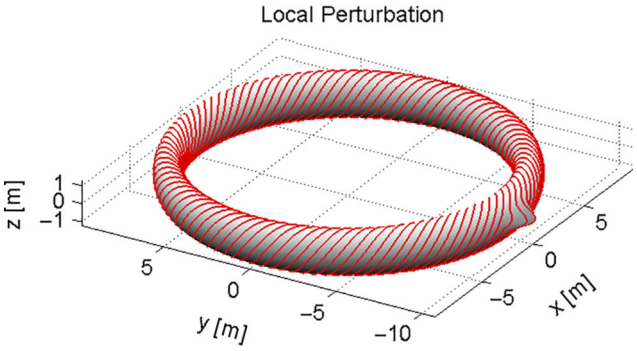

Fig. 6. Ergodic surface covered by a field line for a locally perturbed field configuration.

TABLE II

Tracing Accuracy for MR and RK Estimated Using Clebsch Potentials for an Integration Length of 1000 m with a Step Size of 2.18 mm/T

	$\lvert U-U_0\rvert/U_0$				$\lvert V-V_0\rvert/V_0$				δP (m)			
	Axisymmetric		Global Perturbation		Axisymmetric		Global Perturbation		Axisymmetric		Global Perturbation	
	Local Perturbation		Local Perturbation		Local Perturbation		Local Perturbation		Local Perturbation		Local Perturbation	
MR	8.0e−3	3e−3	4.4e−1		7.0e−3	2.3e−1	2.0e−2		3.0e−4	1.5e−2	8.0e−4	
RK-II	2.3e−5	8.0e−4	2.1e−3		1.3e−5	2.0e−4	4.0e−4		8.9e−7	1.0e−4	4.6e−5	
RK-IV	2.1e−12	1.0e−7	4.3e−8		1.1e−11	2.0e−9	5.3e−9		6.9e−13	4.0e−9	5.5e−9	

Fusion Science and Technology fstfst15-127.3d 1/10/2015 18:46:20

of view. Adaptive ODE solvers might be expected to show better performance than fixed-step integrators in terms of the trade-off between accuracy and computation time; however, the use of step adaptivity may not preserve spatial symmetries with drastic consequences.[10]

IV. APPLICATION TO PLASMA-WALL GAP CALCULATION

In this section, we determine the plasma-wall gap by evaluating 3-D field lines using the RK-IV scheme.

A practical way to reconstruct the plasma boundary of general 3-D field configurations is to define the connection length as the length of the trajectory covered by the plasma particles over an entire magnetic field line up to its eventual intersection to the first wall, from a given starting point; the Larmor radius at this stage is simply neglected. The lines that never intersect the wall (periodic or ergodic) have infinite connection length and are by definition within the plasma, whilst for a finite connection length, they have to be considered outside.[18] By considering a sufficiently dense grid of starting points, it is possible to map the plasma boundary. The problem of tracing infinite length lines can be practically circumvented by assuming that a line is closed when it comes back within a given small distance from the initial point, or by defining a maximum admissible length much higher than expected for lines intersecting the wall.

Following such a connection length approach to the definition of the plasma boundary, we designed a procedure that iteratively calculates the connection length for successive initial positions along a given direction. Once a prescribed accuracy is assigned and a scanning step defined with reference to the expected accuracy, the connection length can be calculated along a segment, for instance, in terms of the distance of the initial point from the wall.

We consider again the reference case as in Sec. III, with now a kink perturbation of 2-deg rotation around the x-axis and a 5-cm shift along the same axis. Referring to such a plasma configuration, the connection lengths of 20 evenly spaced lines were calculated along a radial direction on the midplane in the poloidal plane, from the first wall to the plasma edge, at $\varphi = 0$ and $\varphi = \pi$. Figure 7a shows the r–z values of these field lines, with a blue color map for lines external to the plasma and red for the first internal line. The corresponding Poincaré cross points are shown in Fig. 7b.

Figure 8 shows the connection length in terms of the distance from the first wall for both the considered gaps; a sharp transition from the external region to the plasma region is evident as well as the different distances where it occurs, which is a consequence of the nonaxisymmetric field configuration.

These results can be considered as a proof of principle of the viability of 3-D plasma boundary determination by means of accurate tracing of field lines and evaluation of the connection length. Strategies for an efficient use of computing power can be easily implemented by considering a bisection algorithm for the determination of the plasma-wall gap on the search direction. Parallel computing is also suitable for concurrent calculation of several search directions.[19]

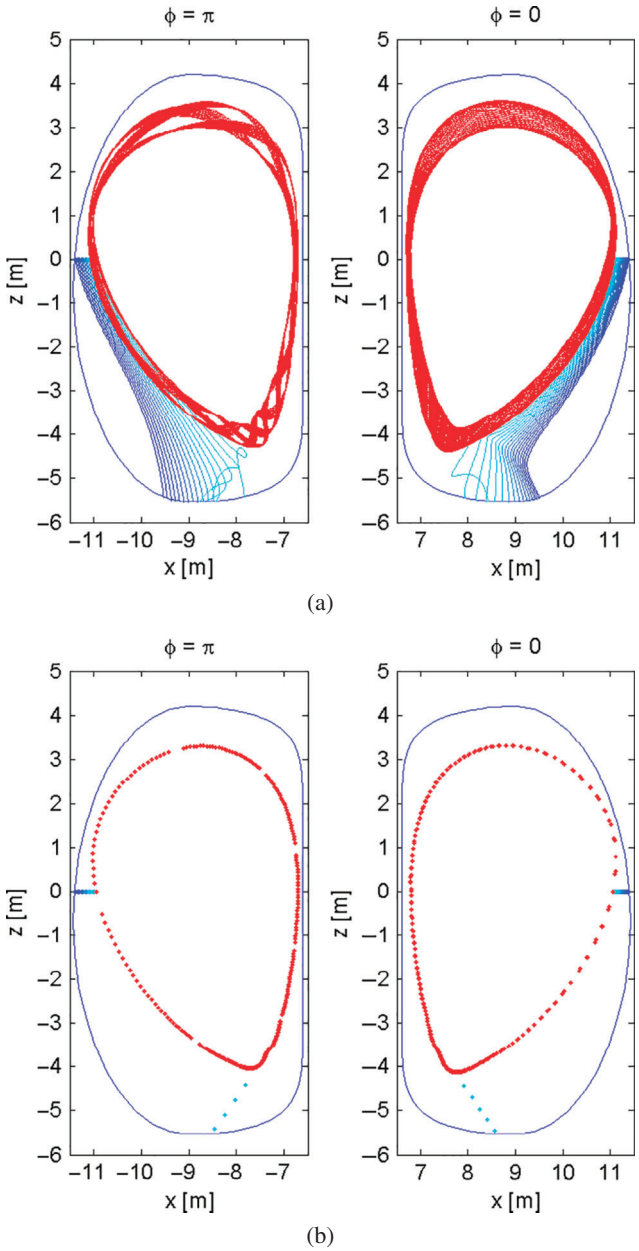

Fig. 7. (a) Three-dimensional field lines in the r–z plane; (b) Poincaré plots of the first internal line at $\varphi = 0$ (right) and $\varphi = \pi$ (left).

V. CONCLUSIONS

We considered the problem of accurate tracing of magnetic field lines in tokamaks, where extremely long

Fusion Science and Technology fstfst15-127.3d 1/10/2015 18:46:20

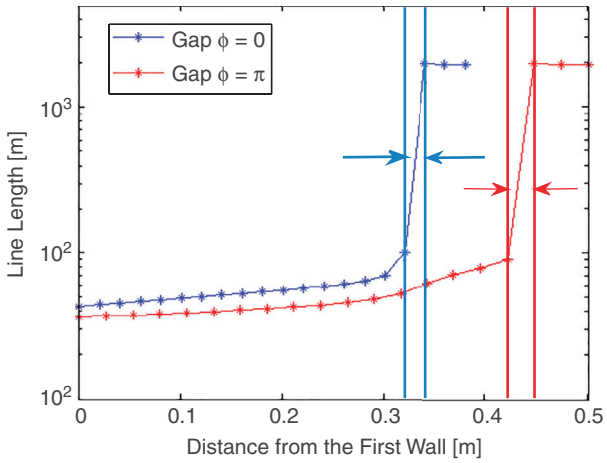

Fig. 8. Connection lengths versus the distance from the first wall on the outboard equatorial plane $z = 0$ at two different toroidal locations (the integration stops after ~2 km).

lines with high local integration accuracy have to be evaluated. A VP ODE solver and standard RK routines were validated and compared with the reference for a specific problem. In particular, the error assessment was conducted by means of analytical invariants, which for the 2-D case are given by the constant poloidal flux values, and for the 3-D case by means of analytical expressions based on Clebsch potentials. Accuracy requirements are met by both integration schemes if the integration step size is adequate. The volume preservation of the RK-IV scheme is comparable to that of the VP scheme when using the same step size, but the overall performance of the RK solver in terms of trade-off in accuracy and computational cost is by far higher than the VP scheme. As a result, standard fixed-step RK integrators are well suited to the problem and can be effectively used for **B**-field tracing in tokamaks. As a demonstration, plasma-wall gaps in a full 3-D configuration were calculated, showing the viability of studying the magnetic properties of plasma boundary in tokamaks using standard tools.

ACKNOWLEDGMENTS

This work was supported in part by the Italian Ministry of Education and Research under grant PRIN-2010SPS9B3. The authors gratefully acknowledge the contribution of A. Guarino in the definition of some test cases.

REFERENCES

1. R. MAINGI et al., "Magnetic Field Line Tracing Calculations for Conceptual PFC Design in the National Compact Stellarator Experiment," *Proc. XXXIII EPS Conf.*, Rome, Italy, June 19–23, 2006.

2. M. W. JAKUBOWSKI et al., "Modelling of the Magnetic Field Structures and First Measurements of Heat Fluxes for TEXTOR-DED Operation," *Nucl. Fusion*, **44**, S1 (2004); http://dx.doi.org/10.1088/0029-5515/44/6/S01.

3. A. PUNJABI and H. ALI, "Symplectic Approach to Calculation of Magnetic Field Line Trajectories in Physical Space with Realistic Magnetic Geometry in Divertor Tokamaks," *Phys. Plasmas*, **15**, 122502 (2008); http://dx.doi.org/10.1063/1.3028310.

4. F. MAVIGLIA et al., "Electromagnetic Models of Plasma Breakdown in the JET Tokamak," *IEEE Trans. Magn.*, **50**, *2*, 937 (2014); http://dx.doi.org/10.1109/TMAG.2013.2282351.

5. M. SHOJI et al., "Investigation of the Helical Divertor Function and the Future Plan of a Closed Divertor for Efficient Particle Control in the LHD Plasma Periphery," *Fusion Sci. Technol.*, **58**, *1*, 208 (2010); http://dx.doi.org/10.13182/FST10-04.

6. T. K. MAU et al., "Divertor Configuration and Heat Load Studies for the ARIES-CS Fusion Plant," *Fusion Sci. Technol.*, **54**, *3*, 771 (2008); http://dx.doi.org/10.13182/FST08-27.

7. A. BRUSCHI et al., "A New Launcher for Real-Time ECRH Experiments on FTU," *Fusion Sci. Technol.*, **55**, *1*, 94 (2009); http://dx.doi.org/10.13182/FST09-27.

8. B. D. BLACKWELL et al., "Algorithms for Real Time Magnetic Field Tracing and Optimization," *Comput. Phys. Commun.*, **142**, 243 (2001); http://dx.doi.org/10.1016/S0010-4655(01)00326-5.

9. R. I. McLACHLAN, G. REINOUT, and G. R. W. QUISPEL, "Geometric Integrators for ODEs," *J. Phys. A: Math. Gen.*, **39**, 5251 (2006); http://dx.doi.org/10.1088/0305-4470/39/19/S01.

10. R. I. McLACHLAN and G. R. W. QUISPEL, "Six Lectures on Geometric Integration," *Foundations of Computational Mathematics*, R. DEVORE, A. ISERLES, and E. SÜLI, Eds., p. 155, Cambridge University Press, Cambridge (2001).

11. J. M. FINN and L. CHACON, "Volume Preserving Integrators for Solenoidal Fields on a Grid," *Phys. Plasmas*, **12**, 054503 (2005); http://dx.doi.org/10.1063/1.1889156.

12. D. BONFIGLIO et al., "Magnetic Chaos Healing in the Helical Reversed-Field Pinch: Indications from the Volume-Preserving Field Line Tracing Code NEMATO," *J. Phys. Conf. Ser.*, **260**, 012003 (2010); http://dx.doi.org/10.1088/1742-6596/260/1/012003.

13. G. CIACCIO et al., "Numerical Verification of Orbit and Nemato Codes for Magnetic Topology Diagnosis," *Phys. Plasmas*, **20**, 062505 (2013); http://dx.doi.org/10.1063/1.4811380.

14. R. ALBANESE et al., "Numerical Formulations for Accurate Magnetic Field Flow Tracing in Fusion Tokamaks," *Proc. 9th IET Int. Conf. Computation in Electromagnetics*, London, United Kingdom, March 31–April 1 (2014); http://dx.doi.org/10.1049/cp.2014.0211.

Fusion Science and Technology fstfst15-127.3d 1/10/2015 18:46:21

15. J. R. DORMAND and P. J. PRINCE, "A Family of Embedded Runge-Kutta Formulae," *J. Comput. Appl. Math.*, **6**, 19 (1980); http://dx.doi.org/10.1016/0771-050X(80)90013-3.

16. G. FEDERICI et al., "Overview of EU DEMO Design and R&D Activities," *Fusion Eng. Des.*, **89**, *7–8*, 882 (2014); http://dx.doi.org/10.1016/j.fusengdes.2014.01.070.

17. S. V. BULANOV et al., "Current Sheet Formation in Three-Dimensional Magnetic Configurations," *Phys. Plasmas*, **9**, 3835 (2002); http://dx.doi.org/10.1063/1.1501093.

18. M. ITAGAKI et al., "Use of a Twisted 3D Cauchy Condition Surface to Reconstruct the Last Closed Magnetic Surface in a Non-Axisymmetric Fusion Plasma," *Plasma Phys. Controlled Fusion*, **54**, 125003 (2012); http://dx.doi.org/10.1088/0741-3335/54/12/125003.

19. R. TSUJI, "Parallel Computing for Tracing Torus Magnetic Field Line," *Proc. Int. Conf. Parallel Computing in Electrical Engineering*, Trois-Rivieres, Quebec, Canada, August 27–30, 2000, IEEE (2000).